



## Generation of waveform-tunable unipolar pulses in a nonlinear resonant medium

Anton Pakhomov <sup>1</sup>, Mikhail Arkhipov,<sup>1</sup> Nikolay Rosanov,<sup>1,2</sup> and Rostislav Arkhipov <sup>1,2</sup>

<sup>1</sup>*St. Petersburg State University, Universitetskaya Nab. 7/9, St. Petersburg 199034, Russia*

<sup>2</sup>*Ioffe Institute, Politekhnikeskaya Str. 26, St. Petersburg 194021, Russia*



(Received 26 August 2022; accepted 20 October 2022; published 7 November 2022)

We theoretically demonstrate the possibility to produce unipolar pulses of varying temporal profile in an extended layer of a resonant medium with the nonlinear coupling to the driving electric field. The proposed approach relies on the coherent control of the low-frequency medium oscillations by a sequence of ultrashort excitation pulses as well as the collective emission of multiple resonant centers along an optically thick medium layer. In particular, we show that creating an inhomogeneous spatial profile of the density of resonant centers allows obtaining unipolar pulses of adjustable waveform, such as rectangular or triangular ones. Such optical response could be realized in Raman-active media, e.g., in molecular crystals with well-resolved vibrational terahertz resonances.

DOI: [10.1103/PhysRevA.106.053506](https://doi.org/10.1103/PhysRevA.106.053506)

### I. INTRODUCTION

Generation of few-cycle pulses in terahertz and especially optical frequency ranges represents one of the major research areas of modern optics [1–4]. The few-cycle pulses allow not only to largely boost the performance of different ultrafast optical systems, e.g., optical data processing and transmission, but also enable efficient control of ultrafast processes in matter, which is inaccessible when using longer multicycle pulses [5–9].

Unipolar pulses can be introduced as a specific case of few-cycle pulses containing just a half of an optical cycle and therefore having a constant sign of the electric field. In a more general case of a sign-varying electric field, unipolar pulses can be defined as those having the nonzero values of the electric pulse area  $\vec{S}_E(\vec{r})$  [10,11]:

$$\vec{S}_E(\vec{r}) = \int_{-\infty}^{+\infty} \vec{E}(\vec{r}, t) dt \neq 0, \quad (1)$$

where  $\vec{E}(\vec{r}, t)$  is the electric field vector. It is worth noting that the electric pulse area Eq. (1) obeys a fundamental conservation law upon the propagation of an arbitrary pulse in any dissipative medium in the one-dimensional (1D) case, so that the electric pulse area stays constant in space [12,13].

Due to their nonzero electric pulse area, Eq. (1) unipolar pulses transfer momentum to charged particles. As the result, unipolar pulses represent a very useful tool for acceleration of charged particles or ionization of atoms [14–16]. Besides that, the nonzero electric pulse area provides an efficient ultrafast nonresonant excitation of electronic states in different resonant media [17–20] or rovibrational levels in polar molecules [21]. Importantly, such nonresonant excitation of higher levels in quantum systems by unipolar pulses exhibits much higher efficiency as compared to usual bipolar pulses with zero electric area Eq. (1), given that the excitation pulse duration is less than the period of the respective

transition [19–21]. Hence, production of unipolar pulses of controllable shape or electric area turns out to be in high demand.

A number of methods have been suggested for generation of unipolar and quasiunipolar subcycle pulses. Those include, among others, the unipolar terahertz pulse formation in a nonequilibrium plasma channel [22,23], excitation of a foil target by intense femtosecond pulses [24–26], generation of attosecond unipolar pulses through cascaded processes in plasma [27], and formation of terahertz unipolar precursor pulses in electro-optical crystals [28–30]. Several possible ways to experimentally determine the unipolarity of the pulsed terahertz radiation were presented in Ref. [31]. Also, a number of papers have theoretically shown the possibility of the unipolar half-cycle soliton formation in different nonlinear media [32–37].

However, in the above papers no ways to control the shape of the produced unipolar pulses were suggested. Still, the issue of shaping of subcycle unipolar pulses is of crucial importance for any applications in all-optical control of ultrafast processes. To the best of our knowledge, just a couple of studies so far have addressed this point. A theoretical approach for the control of the unipolar pulse shape in a layer of a resonant medium with the nonlinear field coupling was proposed in Refs. [38–40], based on varying the geometrical parameters of a thin medium layer and the excitation source. Later, this approach was improved with using diffraction optical elements for the pulse shape control [41]. Nevertheless, the feasibility of these methods is greatly restricted, and efficient methods for obtaining unipolar pulses of controllable waveform are still lacking.

In this paper we propose an efficient approach for the generation of unipolar pulses of tunable waveform from an extended layer of a resonant medium with the nonlinear field coupling, such as a Raman-active medium. Our approach enables producing unipolar pulses of a controllable temporal

profile and duration by means of ultrashort excitation pulses. The tunability of the unipolar pulse waveform is provided through varying the spatial density of the resonant particles along the layer thickness. As the result, unipolar pulses of different unusual shapes can be readily produced, such as rectangular and triangular ones.

This paper is organized as follows. In Sec. II we present the model that we use and show that the response of a thin slice of a resonant medium with the nonlinear field coupling when driven by a pair of exciting ultrashort pulses can be tuned to be a single cycle of a sine wave at medium resonant frequency. In Sec. III it is shown that such response leads to generation of half-cycle unipolar pulses from an extended medium layer due to the constructive interference of the emitted secondary waves from different parts of the layer. In Sec. IV we extend the consideration to optically thick medium layers with nonuniform spatial density and demonstrate that it gives rise to unipolar output pulses of varying shape. Finally, a paper summary and concluding remarks are provided in Sec. V.

## II. MODEL

We assume the induced dipole moment  $p$  of a single resonant center to obey the following equation [40,42]:

$$\ddot{p} + \gamma \dot{p} + \omega_0^2 p = g_0 E(t)^2, \quad (2)$$

with external driving field  $E(t)$ , medium resonant frequency  $\omega_0$  and damping rate  $\gamma$ , and the nonlinear coupling factor to the driving field  $g_0$ . As it was demonstrated in Ref. [42], the simple model Eq. (2) is well suited for the description of the low-frequency response of a Raman-active medium upon its excitation by ultrashort pulses of subpicosecond duration. Indeed, the optical response of a molecular Raman-active medium can be carefully modeled when assuming the medium consisting of two nonlinearly coupled harmonic oscillators—a high-frequency (electronic) oscillator (HFO) and low-frequency (nuclear) oscillator (LFO) [43,44]. If  $y$  stands for the normal coordinate of LFO oscillations and  $x$  stands for the normal coordinate of HFO oscillations, the dynamics of a Raman-active medium under a pulsed excitation is driven by the following system of coupled equations [43,44]:

$$\ddot{x} + \Gamma_e \dot{x} + \Omega_0^2 x = -\frac{q}{m} E(t) - \frac{\gamma}{m} xy, \quad (3)$$

$$\ddot{y} + \Gamma_n \dot{y} + \omega_0^2 y = -\frac{\gamma}{2M} x^2. \quad (4)$$

The parameters of the model are the following:  $M$  and  $m$  are the effective masses of the LFO and HFO,  $\Gamma_e$  and  $\Gamma_n$  are the damping rates of HFO and LFO, factor  $\gamma$  is the strength of the nonlinear coupling between HFO and LFO,  $q$  is the effective charge of both oscillators,  $\omega_0 = 2\pi/T_0$  is the resonant frequency of the LFO, and  $\Omega_0 = 2\pi/T_\Omega$  is the resonant frequency of the HFO. As a specific example of a Raman-active medium governed by Eqs. (3) and (4), one can take molecular crystals which typically possess isolated vibrational resonances in the terahertz range [45].

The model Eq. (2) makes use of the following expansion of the binding potential energy:

$$U(x, y) = \frac{m\Omega_0^2}{2} x^2 + \frac{M\omega_0^2}{2} y^2 + \frac{\gamma}{2} x^2 y, \quad (5)$$

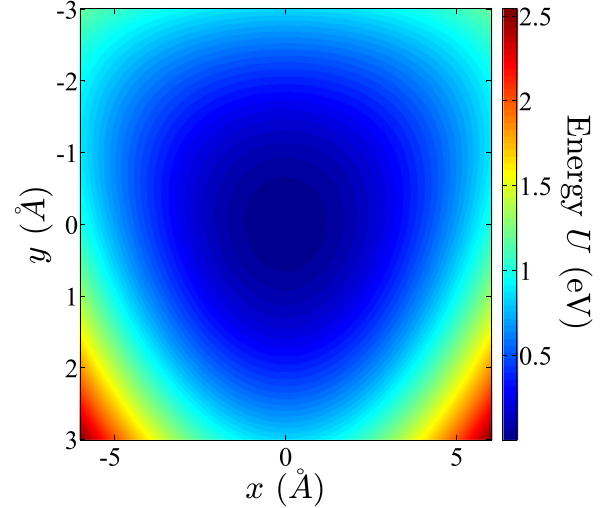


FIG. 1. An exemplary plot of the potential energy distribution  $U(x, y)$  for a system of two nonlinearly coupled oscillators given by Eq. (5). The model parameters are the effective masses  $M = 3 \times 10^{-26}$  kg and  $m = 9.1 \times 10^{-31}$  kg, resonant frequencies  $\omega_0 = 10^{13}$  s $^{-1}$  and  $\Omega_0 = 10^{15}$  s $^{-1}$ , and coupling strength  $\gamma = 10^9$  J/m $^3$ .

where the last coupling term introduces spatial asymmetry into the system and is eventually responsible for the nonlinear coupling of the low-frequency induced medium polarization to the driving electric field as described by Eq. (2). The potential energy Eq. (5) for some exemplary parameter values is plotted in Fig. 1. One can easily see the asymmetry arising due to the nonlinear bonding term. In fact, according to Eq. (3), the slow oscillations of LFO effectively cause the gradual change of the HFO resonant frequency, which is also manifested in changing the parabolic slope  $U(x)$  in the potential energy profile for different  $y$  coordinates in Fig. 1. On the other hand, the LFO oscillations are driven by an external force term of the constant sign, whose frequency is mainly determined by the frequency of the pumping electric field, namely, the doubled pumping frequency. As a result, the induced medium polarization,

$$P = Nq(y - x),$$

where  $N$  is the spatial density of resonant particles, primarily contains the spectral contributions at the LFO and HFO resonant frequencies as well as pumping frequency (including nearby Stokes and anti-Stokes lines) and its second harmonic. If the pumping frequency is much larger than LFO resonant frequency, the LFO emission can be easily obtained using a low-pass filter that cuts off all contributions both from the pumping pulse and the HFO oscillations. The remaining low-frequency part of the induced medium polarization can be then well described by Eq. (2) [42].

Let us now proceed with the possibilities to perform coherent control of the low-frequency medium polarization oscillations. Following the findings in Ref. [42], we suppose that the resonant medium Eq. (2) is excited by a pair of ultrashort pulses:

$$E(t) = E_0 e^{-t^2/\tau_p^2} \sin \Omega_p t + E_0 e^{-(t-\Delta)^2/\tau_p^2} \sin \Omega_p (t - \Delta), \quad (6)$$

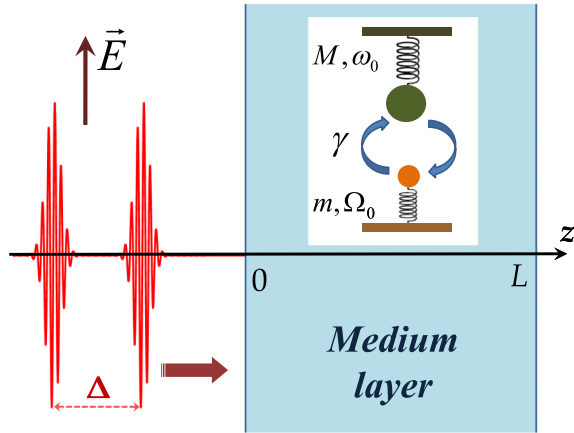


FIG. 2. Sketch of the system under consideration: a pair of linearly polarized ultrashort pulses hits an extended layer of a medium with nonlinearly coupled resonances, as provided by Eqs. (3) and (4).

with the electric field amplitude  $E_0$ , excitation pulse duration  $\tau_p$ , carrier frequency  $\Omega_p$ , and pulse-to-pulse delay  $\Delta$ . It is supposed that the pumping frequency  $\Omega_p$  is far from both resonant frequencies  $\omega_0$  and  $\Omega_0$ , so that we can reliably neglect the dynamics of the population inversion. The time delay between pulses  $\Delta$  is selected to equal

$$\Delta = \frac{T_0}{2} = \frac{\pi}{\omega_0}, \quad (7)$$

i.e., half of the period of the resonant medium oscillations [42]. Such a choice ensures the efficient coherent control of the induced low-frequency medium polarization through the excitation pulses. Namely, as the first excitation pulse Eq. (6) initiates the oscillations of the induced dipole moments according to Eq. (2) at the resonant frequency  $\omega_0$ , the second excitation pulse stops these oscillations after a half period, provided that the pulse-to-pulse delay obeys Eq. (7). As a result, the induced dipole moment represents a half-sine wave [42].

We now assume that a pair of excitation pulses Eq. (6) is incident on a thick layer of the resonant nonlinear medium Eq. (2) of thickness  $L$ :

$$L \gg \lambda_0, \quad (8)$$

where  $\lambda_0$  is the wavelength of the resonant transition, i.e.,  $\lambda_0 = cT_0 = 2\pi c/\omega_0$ , with the speed of light  $c$ . The pulses are taken linearly polarized. Besides that, we consider the case of the normal incidence, as sketched in Fig. 2. Under these assumptions the problem reduces to a 1D one and can be described by the scalar 1D wave equation for the electric field  $E(z, t)$ :

$$\frac{\partial^2 E(z, t)}{\partial z^2} - \frac{1}{c^2} \frac{\partial^2 E(z, t)}{\partial t^2} = \frac{4\pi}{c^2} \frac{\partial^2 P(z, t)}{\partial t^2}, \quad (9)$$

which must be coupled to the equation describing the response of the nonlinear medium Eq. (2). The one-dimensional approximation was also demonstrated to be well justified for the few- and subcycle pulse propagation in coaxial waveguides [10]. The bulk medium polarization in the right-hand side of Eq. (9) is readily obtained from the induced dipole

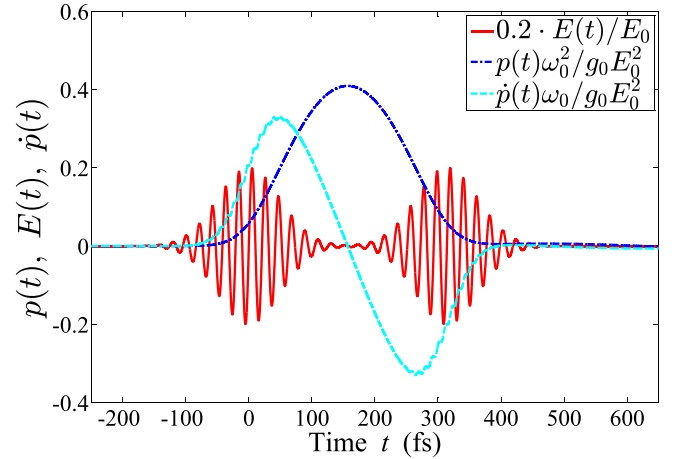


FIG. 3. Optical response of a single resonant center of a nonlinear medium driven by Eq. (2) together with the driving electric field Eq. (6). All quantities are accordingly rescaled and plotted in dimensionless units. The medium's resonant frequency is  $\omega_0 = 10^{13} \text{ s}^{-1}$ , damping rate  $\gamma = 10^{11} \text{ s}^{-1}$ , excitation pulse duration  $\tau_p = 70 \text{ fs}$ , and carrier frequency  $\Omega_p = 3 \times 10^{14} \text{ s}^{-1}$ .

moment of a single resonant center Eq. (2) as

$$P(z, t) = N(z) p(z, t), \quad (10)$$

with the spatial density of the resonant atoms/molecules  $N(z)$ , which is in general spatially varying.

For the field emitted by a medium layer in a one-dimensional problem, the following exact solution of Eq. (9) can be derived [46]:

$$E_{\text{emit}}(z, t) = -\frac{2\pi}{c} \int_0^L \frac{\partial P(z', t - \frac{|z-z'|}{c})}{\partial t} dz'. \quad (11)$$

According to Eq. (11), the optical response of the layer is determined by the first-order temporal derivative of the induced medium polarization, instead of the second-order temporal derivative in a three-dimensional geometry [47].

In Fig. 3 we have plotted the results of the excitation of a single resonant center described by Eq. (2) when driven by the pulses of Eq. (6). Specifically, we plot the temporal dependence of the induced dipole moment  $p(t)$  and its temporal derivative together with the driving electric field Eq. (6). It is well seen that due to the choice of the interspike delay Eq. (7), the second excitation pulse indeed fully stops the resonant oscillations of the induced dipole moment, initiated by the first excitation pulse, after a half of the oscillation cycle. It should be noted that the strength of the induced dipole moment  $p(t)$  linearly depends on the product  $g_0 E_0^2$  according to Eq. (2), which is why we use dimensionless values in Fig. 3 without loss of generality.

At the same time, the temporal derivative of the induced dipole moment  $\dot{p}(t)$  in Fig. 3 makes a single oscillation cycle and can be well approximated by one period of the sine wave. The shape of the temporal derivative  $\dot{p}(t)$  largely depends on the duration of the excitation pulses  $\tau_p$ . If the pulse duration  $\tau_p$  is much smaller than the time delay Eq. (7), the temporal derivative  $\dot{p}(t)$  would possess sharp jumps at the moments of both pulses' action. When increasing the pulse duration  $\tau_p$  to

become comparable with the time delay Eq. (7), one ends up with a relatively smooth profile of  $\dot{p}(t)$ , like the one shown in Fig. 3.

According to Eq. (11) the temporal dependence of the derivative of the induced dipole moment  $\dot{p}(t)$  in Fig. 3 also describes the emitted field from a very thin flat layer of the nonlinear medium Eq. (2) [42]. To be more specific, the layer thickness in this case has to be much smaller than the wavelength of the resonant transition, i.e., exactly opposite to the inequality Eq. (8). Provided that the emitted field Eq. (11) is much smaller in amplitude than the field of the incident pulses, the temporal derivative of the induced medium polarization in Eq. (11), i.e., the layer emission, is just the product of the temporal derivative  $\dot{p}(t)$  for a single resonant center times the spatial density of resonant centers in the layer.

### III. GENERATION OF HALF-CYCLE UNIPOLAR PULSES

Let us now consider the response of an optically thick layer with a spatially dependent density  $N(z)$ . Following the results of the previous section, we can reliably accept that each infinitesimal slice of the resonant medium  $\delta z$  emits a single-cycle pulse at their resonant frequency  $\omega_0$ , i.e.,

$$A(z, t)|_{z=-D} = A_0(z)\delta z \sin \omega_0 \left( t - \frac{2z+D}{c} \right),$$

$$\frac{2z+D}{c} \leq t \leq \frac{2z+D}{c} + T_0, \quad (12)$$

with the respective field amplitude  $A_0(z)$  and the distance  $D$  between the left boundary of the medium layer and the detector, i.e., the detecting system is assumed located at the point  $z = -D$ . The emitted field is therefore measured in the reflection. This choice appears suitable, since in transmission the layer emission interferes with the excitation pulses Eq. (6), while in reflection one only detects the layer emission. We also suppose that the field Eq. (12) corresponds to the unity value of the spatial density of resonant particles in the layer.

It is assumed in Eq. (12) that at the time point  $t = 0$  the first of the excitation pulses reaches the left boundary of the layer in Fig. 2. Starting from this moment, it takes for the excitation pulses the amount of time  $z/c$  to reach the resonant particle located at the point  $z$  and then it takes for the emitted field from this resonant particle the amount of time  $(z+D)/c$  to reach the detector. This clarifies the boundaries of the time slot in Eq. (12) for the detected radiation from each specific slice of the layer. Here, for the sake of simplicity, we assume the refractive index of the host medium to be equal to unity both at the pump frequency and at the emission frequency, which is justified for low enough density values. In an arbitrary case one would have to replace the speed of light with the respective group velocities in Eq. (12), which would only change the factor in front of  $z$  in Eq. (12) without affecting the main findings below. Also, the contribution of the resonant centers Eq. (2) to the refractive index must be negligible, so that the inhomogeneity of the spatial density  $N(z)$  does not lead to the spatially dependent group refractive index of light.

In order to calculate the emitted field from the whole layer, one has to sum up all responses Eq. (12) over the thickness of the layer, where the time delays have to be correctly taken

into account. Hence the total layer's response is given as

$$E(-D, t) = \int_0^L N(z)A(z, t)dz, \quad (13)$$

with the spatial density  $N(z)$ .

Let us start with the simplest case, namely, a uniform spatial density  $N(z) = N_0$ . We also neglect here the spatial dependence of  $A_0(z)$  in Eq. (12), assuming the excitation pulses negligibly transform over their propagation in the layer, so that each medium's resonant center gets excited by the same pulses Eq. (6). In this case, when both excitation pulses have entered the medium layer, Eq. (13) yields

$$E(-D, t) = N_0 A_0 \int_{(ct-D-\lambda_0)/2}^{(ct-D)/2} \sin \omega_0 \left( t - \frac{2z+D}{c} \right) dz = 0,$$

$$\frac{D+\lambda_0}{c} \leq t \leq \frac{D+2L}{c}, \quad (14)$$

i.e., we get no emitted field. This result arises due to the destructive interference of the emitted fields from different slices over the whole layer thickness. Indeed, according to the findings of the previous section, every infinitesimal medium slice emits a single-cycle pulse Eq. (12). If the spatial density  $N(z)$  does not change over the layer thickness, the positive and negative half-waves from different parts of the medium layer will fully compensate each other, resulting in zero total field.

Equation (14) was obtained with the specific choice of the harmonic emitted field Eq. (12). However, it can be shown that zero emitted field for a uniform spatial density  $N(z) = N_0$  would be detected for an arbitrary profile of the resonant center's emission instead of Eq. (12). Let us replace Eq. (12) with a certain other odd function  $f$ :

$$A(z, t)|_{z=-D} = A_0(z)\delta z \cdot f \left( t - \frac{2z+D}{c} \right),$$

$$\frac{2z+D}{c} \leq t \leq \frac{2z+D}{c} + T_0,$$

$$f \left( \frac{2z+D}{c} \right) = f \left( \frac{2z+D}{c} + T_0 \right) = 0,$$

$$f \left( \frac{2z+D}{c} + \frac{T_0}{2} + \tau \right) = -f \left( \frac{2z+D}{c} + \frac{T_0}{2} - \tau \right),$$

$$\text{for } 0 \leq \tau \leq \frac{T_0}{2}. \quad (15)$$

The exact shape of the function  $f(t)$  mainly depends on the ratio between the excitation pulse duration  $\tau_p$  and the delay Eq. (7). In any case, however, the function  $f(t)$  has to be equal to zero before the action of the first excitation pulse and after the action of the second excitation pulse due to the selected value of the delay Eq. (7). Besides that, since Eq. (2) yields the free resonant oscillations in between the excitation pulses, function  $f(t)$  has to be uneven vs time measured from the central time point in between the excitation pulses Eq. (6). This reasoning explains the imposed restrictions on the function  $f(t)$  in Eq. (15).

Using the emission in the form of Eq. (15), Eq. (13) yields the following for the total emitted field, when both excitation



pulses have entered the medium layer:

$$E(-D, t) = N_0 A_0 \int_{(ct-D-\lambda_0)/2}^{(ct-D)/2} f\left(t - \frac{2z+D}{c}\right) dz \\ \sim \int_{-T_0/2}^{T_0/2} f\left(\tau' + \frac{T_0}{2}\right) d\tau' = 0,$$

$$\text{where } \tau' = t - \frac{2z+D}{c} - \frac{T_0}{2}, \\ \frac{D+\lambda_0}{c} \leq t \leq \frac{D+2L}{c}.$$

Hence, due to the symmetry properties of the function  $f(t)$  the destructive interference of the emitted fields from different slices of the medium layer results in zero emitted field regardless of the specific shape of the function  $f(t)$ .

This result, however, holds only in the central part of the reflected signal. Specifically, when the first excitation pulse has already entered the medium layer while the second pulse has not, instead of Eq. (14), one gets another expression from Eq. (13) with the response in the form Eq. (12):

$$E(-D, t) = N_0 A_0 \int_0^{(ct-D)/2} \sin \omega_0 \left(t - \frac{2z+D}{c}\right) dz \\ = \frac{A_0 N_0 \lambda_0}{4\pi} \left[1 - \cos \omega_0 \left(t - \frac{D}{c}\right)\right], \\ \frac{D}{c} \leq t \leq \frac{D+\lambda_0}{c}. \quad (16)$$

Equation (16) describes a half-cycle unipolar pulse arising at the very leading edge of the layer emitted field due to the constructive interference of the fields Eq. (12) from the resonant particles located near the left boundary of the medium layer. Exactly the same unipolar half-cycle pulse but of opposite polarity appears at the very trailing edge, when the first excitation pulse has already left the medium layer while the second pulse has not:

$$E(-D, t) = N_0 A_0 \int_{(ct-D-\lambda_0)/2}^L \sin \omega_0 \left(t - \frac{2z+D}{c}\right) dz \\ = -\frac{A_0 N_0 \lambda_0}{4\pi} \left[1 - \cos \omega_0 \left(t - \frac{D+2L}{c}\right)\right], \\ \frac{D+2L}{c} \leq t \leq \frac{D+2L+\lambda_0}{c}. \quad (17)$$

Hence the measured signal in reflection represents a pair of half-cycle unipolar pulses following with a significant time delay between them. According to Eq. (14), this time delay is given as  $(2L + \lambda_0)/c \approx 2L/c$ , i.e., linearly proportional to the layer thickness. Therefore it is possible to obtain effectively isolated unipolar half-cycle pulses, if this time delay is tuned to be large enough.

Figure 4 shows an example of the reflected electric field from an extended layer of the nonlinear resonant medium Eq. (2) with the uniform spatial density  $N(z) = N_0$  calculated through the direct numerical solution of the coupled equations Eqs. (2), (9), and (10). For numerical simulations we used the finite-difference time-domain method (FDTD) for the wave equation Eq. (9), while Eq. (2) was solved with the high-order Runge-Kutta method. The calculated emitted

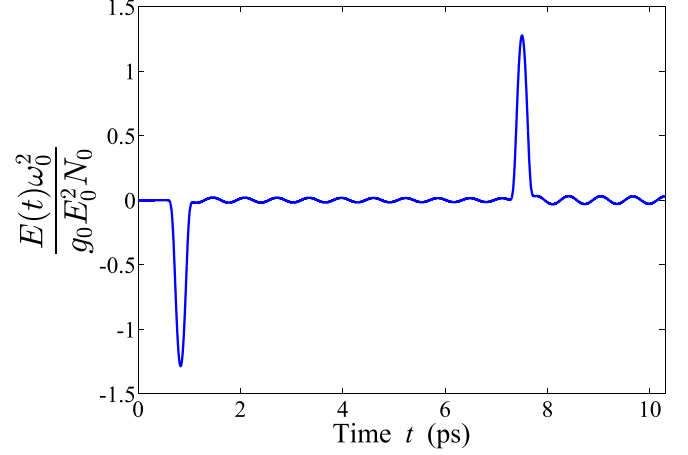


FIG. 4. Rescaled electric field obtained in reflection from an extended layer of the nonlinear resonant medium Eq. (2) with the spatially homogeneous density, with layer thickness  $L = 1$  mm, resonant frequency  $\omega_0 = 10^{13} \text{ s}^{-1}$ , damping rate  $\gamma = 10^{11} \text{ s}^{-1}$ , density of resonant centers  $N_0 = 10^{18} \text{ cm}^{-3}$ , the duration of the exciting pulses  $\tau_p = 70$  fs, and carrier frequency  $\Omega_p = 3 \times 10^{14} \text{ s}^{-1}$ .

field exactly matches the analytical findings above, with two separated-in-time, half-cycle unipolar pulses and a near-zero field between them. It should also be noted that a similar response was recently obtained from a layer of a two-level medium in Ref. [48], but only with unipolar excitation pulses.

In fact, the electric field in the central part of the reflected signal between half-cycle unipolar pulses does not exactly equal zero, and some small oscillations still appear. The reason for that is the non-negligible distortion of both excitation pulses upon their propagation through an extended medium layer. As a result, the amplitude of the excitation pulses slightly decreases towards the right boundary of the medium layer. Therefore the amplitude of the single-cycle pulse from each thin slice of the layer  $A_0(z)$  in Eq. (12) also in turn gradually monotonously decreases with  $z$ . This leads to the slight deviations from the complete mutual compensation of the fields emitted from different parts of the layer in Eq. (14) and the remaining field oscillations between half-cycle unipolar pulses at the edges of the medium response. Similar field oscillations arise for the same reason also behind the second half-cycle unipolar pulse, i.e., at the trailing edge of the reflected field, as can be seen in Fig. 4.

As long as the amplitude of the emitted field is orders-of-magnitude weaker than the amplitude of the excitation pulses, the medium response can be taken linearly proportional to the product  $g_0 E_0^2$ . That is why we used rescaled values in Fig. 4. In this case the amplitude of the remaining weak field oscillations is primarily determined by the density of the resonant particles  $N_0$ . At the same time, the strengths of unipolar pulses in Fig. 4 are still linearly proportional to  $N_0$ , which also allows rescaling the emitted field by the  $N_0$  factor. On the other hand, the strength of the remaining low-amplitude oscillations of the emitted field in Fig. 4 does depend on the particle density  $N_0$ , with larger values of  $N_0$  leading to stronger field oscillations, so that one has to keep in mind the specific values of  $N_0$  for each specific figure of the emitted field.

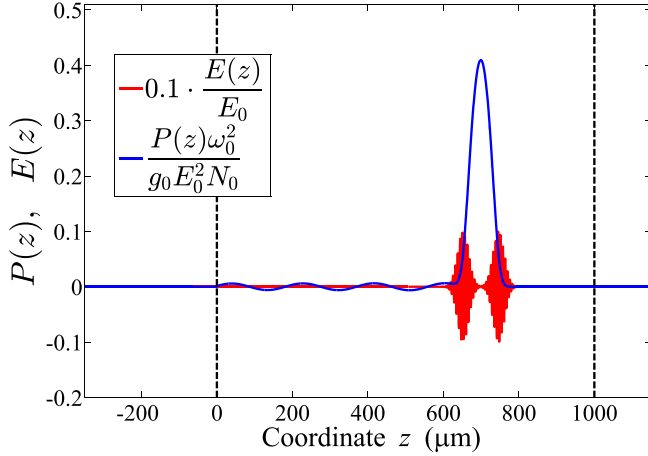


FIG. 5. Instantaneous spatial distribution of the rescaled induced medium polarization inside an extended layer of the nonlinear resonant medium Eq. (2) with the spatially homogeneous density together with the respective rescaled electric field. The picture is taken at a moment when both excitation pulses are still propagating inside the medium layer, black vertical dashed lines indicate the boundaries of the medium layer, and all parameters are the same as in Fig. 4.

It seems convenient to illustrate also the dynamics of the induced medium polarization. In Fig. 5 we have plotted an instantaneous distribution of the medium polarization  $P(z, t)$  at a certain time point, when both excitation pulses still propagate inside the medium layer. For clarity, the corresponding instantaneous distribution of the electric field is also shown.

In Fig. 5 one can see the polarization dynamics described in the previous section for a single resonant center, namely, that the first excitation pulse initiates the induced polarization oscillations at the medium resonant frequency, while the second pulse stops these oscillations after a half cycle. Such control of polarization oscillations is again enabled through the choice of the time delay between excitation pulses given by Eq. (7), since only in this case can the second excitation pulse fully stop the induced polarization oscillations.

However, in contrast to the treatment in the previous section, now we observe such polarization dynamics in a spatially extended layer of the resonant medium Eq. (2). That is why we can see in Fig. 5 a half cycle of the medium polarization, which is placed right in between two excitation pulses and propagates along the medium together with them. Such a traveling half-cycle burst of the medium polarization then produces the layer emission following Eq. (11). In particular, when both excitation pulses are inside the medium layer, Eq. (11) has to yield zero emitted field, as the emission from the leading edge of the polarization burst with the growing polarization would be fully compensated by the emission from the trailing edge of the polarization burst with the decreasing polarization. The nonzero bursts of the electric field are to be emitted only at the leading and trailing edges of the medium response, when the half-cycle burst of the medium polarization in Eq. (11) is just arising or vanishing, respectively. This reasoning is in full agreement with the results of Eqs. (14)–(17) and the numerically calculated field in Fig. 4. It

should be also noted that some small polarization oscillations are well seen in Fig. 5 left behind the polarization burst, which are eventually responsible for the remaining low-amplitude field oscillations in Fig. 4.

#### IV. WAVEFORM-TUNABLE UNIPOLAR PULSES

The treatment above was based on the assumption of a spatially uniform density distribution of the resonant centers along the medium layer. We proceed, therefore, with the inhomogeneous spatial density. Different spatial profiles of the density distribution could be made, for example, using mature techniques of controlling the three-dimensional arrangement of guest molecules upon growth of multicomponent molecular crystals or organic semiconductors [49]. First we take the linear dependence of the spatial density  $N(z)$  on the coordinate:

$$N(z) \sim z.$$

To be more specific, we will focus on a symmetric profile, so that

$$N(z) = 2N_0 \frac{z}{L}, \quad 0 \leq z \leq \frac{L}{2},$$

$$N(z) = 2N_0 \frac{L-z}{L}, \quad \frac{L}{2} \leq z \leq L, \quad (18)$$

with the maximum density value  $N_0$  at the center of the layer and the layer thickness  $L$ . Given that, Eq. (13) for the emitted field yields for the emission of the left half of the layer, i.e., the one with the increasing density,

$$E(-D, t) = \frac{2N_0 A_0}{L} \int_{(ct-D-\lambda_0)/2}^{(ct-D)/2} z \sin \omega_0 \left( t - \frac{2z+D}{c} \right) dz$$

$$= \frac{A_0 N_0 \lambda_0^2}{4\pi L} = \text{const},$$

$$\frac{D+\lambda_0}{c} \leq t \leq \frac{D+L}{c}, \quad (19)$$

so we get a constant electric field value, i.e., the rectangular unipolar pulse. Similarly, the right half of the layer Eq. (18) would generate an identical rectangular unipolar pulse but of the opposite sign of the electric field. At the same time, at the leading edge of the emitted signal Eq. (13) gives

$$E(-D, t) = \frac{2N_0 A_0}{L} \int_0^{(ct-D)/2} z \sin \omega_0 \left( t - \frac{2z+D}{c} \right) dz$$

$$= \frac{A_0 N_0 \lambda_0}{4\pi L} (ct-D) - \frac{A_0 N_0 \lambda_0^2}{8\pi^2 L} \cdot \sin \omega_0 \left( t - \frac{D}{c} \right),$$

$$\frac{D}{c} \leq t \leq \frac{D+\lambda_0}{c},$$

i.e., due to the continuous distribution of the spatial density Eq. (18) instead of the field bursts as in Eqs. (16) and (17) we get a smooth monotonously increasing field from zero until the value Eq. (19).

The respective results of the numerical simulations for the reflected field are shown in Fig. 6. In addition, we also plot in the same figure the emitted field for the case of the trapezoidal profile of the spatial density, when the spatial density  $N(z)$  linearly increases or decreases in the left and right thirds of the layer, while in the central third the spatial density is uniform

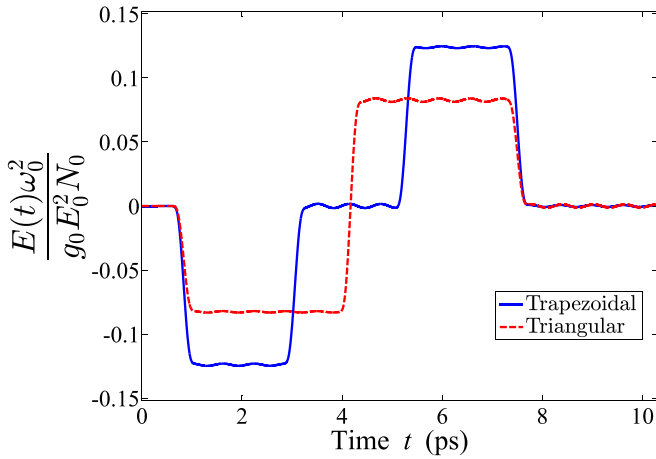


FIG. 6. Rescaled electric field obtained in reflection from an extended layer of the nonlinear resonant medium Eq. (2) with the triangular and trapezoidal profile of the spatial density distribution. The largest value of the density of resonant centers  $N_0 = 10^{18} \text{ cm}^{-3}$ , and other parameters are the same as in Fig. 4.

and equals  $N_0$ . Both profiles of the spatial density distribution are plotted for clarity among others in Fig. 7. One can see that with the trapezoidal density profile the emitted field again consists of two rectangular unipolar pulses of opposite polarity, but now separated in time by a near-zero field plateau. The amplitude of the rectangular unipolar pulses is increased as compared to the triangular density profile, since this amplitude according to Eq. (19) is proportional to the slope of the spatial density, which is larger for the trapezoidal profile in Fig. 7. One can easily see that the time delay between two rectangular unipolar pulses for the trapezoidal density profile grows as one increases the length of the central uniform part in the spatial density distribution. As a result, one can obtain two unipolar pulses with largely tunable time delay between them, which should enable their separation in order to have an isolated rectangular unipolar pulse.

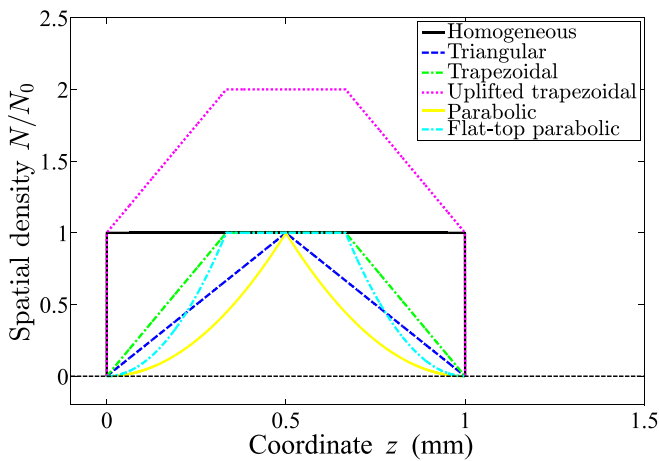


FIG. 7. Different considered profiles of the spatial density distribution  $N(z)$  inside an extended layer of the nonlinear resonant medium Eq. (2); the layer thickness  $L = 1 \text{ mm}$ .

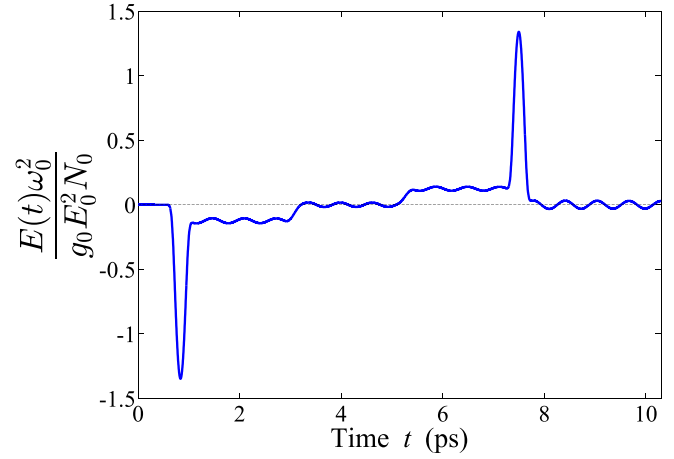


FIG. 8. Rescaled electric field obtained in reflection from an extended layer of the nonlinear resonant medium Eq. (2) with the trapezoidal profile of the spatial density distribution. The lowest value of the density of resonant centers  $N_0 = 10^{18} \text{ cm}^{-3}$ , while the largest value in the central part equals  $2N_0$ ; other parameters are the same as in Fig. 4.

Different profiles of the spatial density distribution  $N(z)$  inside an extended medium layer are summarized in Fig. 7. Here for triangular and parabolic profiles the spatial density first increases from zero at the layer's left boundary to the layer's center and then decreases similarly from the layer's center until its right boundary. In contrast, in cases of trapezoidal and flat-top parabolic profiles the layer length is divided into three equal parts, where in the left and right parts the spatial density again increases and decreases, while in the central part the spatial density stays constant.

Since the resonant particle density can be hard to reduce to zero at the boundaries, we additionally examine the case of a trapezoidal-shaped profile  $N(z)$  but with nonzero density values at the layer boundaries. Specifically, we select the following expression for  $N(z)$ :

$$\begin{aligned}
 N(z) &= N_0 \left( 1 + \frac{3z}{L} \right), & 0 \leq z \leq \frac{L}{3}, \\
 N(z) &= 2N_0, & \frac{L}{3} \leq z \leq \frac{2L}{3}, \\
 N(z) &= N_0 \left( 1 + \frac{3(L-z)}{L} \right), & \frac{2L}{3} \leq z \leq L.
 \end{aligned} \quad (20)$$

The respective profile is also shown in Fig. 7, where we denote it as the uplifted trapezoidal one. The generated field in reflection for this case is plotted in Fig. 8. As could be expected, the obtained field is close to the simple linear superposition of the fields generated in the case of the homogeneous profile in Fig. 4 and in the case of the trapezoidal profile in Fig. 6. The temporal shape of the produced unipolar pulses appears to be quite irregular, since the amplitudes of half-cycle unipolar bursts at the edges of the emitted field are almost by an order of magnitude stronger than the amplitudes of rectangular unipolar parts.

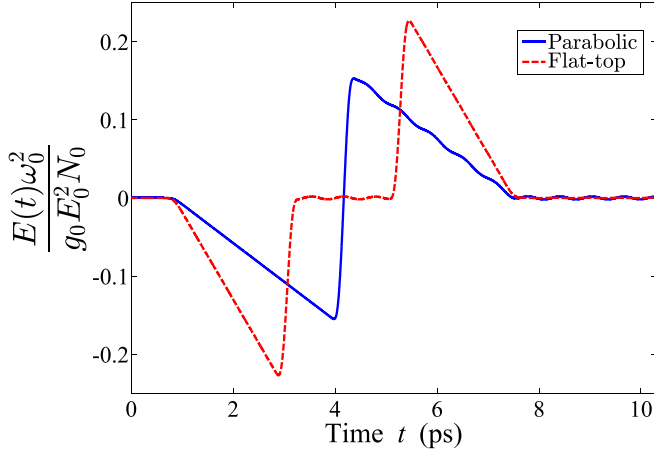


FIG. 9. Rescaled electric field obtained in reflection from an extended layer of the nonlinear resonant medium Eq. (2) with the parabolic profile of the spatial density distribution, either with or without a flat-top section. The largest value of the density of resonant centers is  $N_0 = 10^{18} \text{ cm}^{-3}$ ; other parameters are the same as in Fig. 4.

Next, we proceed with the parabolic dependence of the spatial density  $N(z)$ :

$$N(z) \sim z^2.$$

As before, we take a symmetric profile:

$$\begin{aligned} N(z) &= 4N_0 \frac{z^2}{L^2}, & 0 \leq z \leq \frac{L}{2}, \\ N(z) &= 4N_0 \frac{(L-z)^2}{L^2}, & \frac{L}{2} \leq z \leq L, \end{aligned} \quad (21)$$

which is illustrated in Fig. 7. Now, applying Eq. (13), we find the following for the emitted field from the left half of the layer, i.e., with the quadratically increasing density:

$$\begin{aligned} E(-D, t) &= \frac{4N_0 A_0}{L^2} \int_{(ct-D-\lambda_0)/2}^{(ct-D)/2} z^2 \sin \omega_0 \left( t - \frac{2z+D}{c} \right) dz \\ &= \frac{A_0 N_0 \lambda_0^2}{2\pi L^2} (ct - D - \lambda_0/2), \\ \frac{D + \lambda_0}{c} &\leq t \leq \frac{D + L}{c}, \end{aligned} \quad (22)$$

i.e., the electric field linearly grows with time, which corresponds to a triangular-shaped unipolar pulse. The right half of the layer Eq. (21) with the quadratically decreasing density  $N(z)$  would again emit an identical triangular-shaped unipolar pulse but of the opposite sign of the electric field.

In Fig. 9 we have depicted the respective results of the numerical simulations for the emitted field in reflection. One can see two sequential triangular unipolar pulses of opposite sign. In order to get these triangular unipolar pulses shifted in time, we can turn to the flat-top parabolic density profile:

$$N(z) = 9N_0 \frac{z^2}{L^2}, \quad 0 \leq z \leq \frac{L}{3}, \quad N(z) = N_0, \quad \frac{L}{3} \leq z \leq \frac{2L}{3}, \quad (23)$$

$$N(z) = 9N_0 \frac{(L-z)^2}{L^2}, \quad \frac{2L}{3} \leq z \leq L, \quad (24)$$

which is also illustrated in Fig. 7. As a result, we obtain instead two triangular unipolar pulses with the time delay between them linearly proportional to the length of the flat-top central section of the density profile. Hence, it is possible to get an effectively isolated triangular unipolar pulse by increasing the layer thickness and thus the time delay between both unipolar pulses.

We can eventually consider the more general case of an arbitrary power-law dependence of the spatial density  $N(z)$ :

$$N(z) \sim z^n.$$

Equation (13) then yields the following for the emitted field:

$$E(-D, t) \sim \int_{(ct-D-\lambda_0)/2}^{(ct-D)/2} z^n \sin \omega_0 \left( t - \frac{2z+D}{c} \right) dz. \quad (25)$$

One can easily see that the leading term in the temporal field dependence given by the integral Eq. (25) is  $\sim t^{n-1}$ . Therefore it is possible to tune the profile of produced unipolar pulses in wide limits to an arbitrary power-law dependence through adjusting the spatial density profile  $N(z)$ .

Finally, we want to take a look at the role of the symmetry of the density distribution. Indeed, all the considered profiles  $N(z)$  in Fig. 7 possess symmetry with respect to the layer center, resulting in similar symmetry of the obtained unipolar pulses. Let us now consider the case when the spatial density changes monotonously over the layer thickness. Specifically, we take here the linearly growing profile  $N(z)$ , i.e.,

$$N(z) = N_0 \frac{z}{L}, \quad 0 \leq z \leq L. \quad (26)$$

The emitted field in this case has to follow Eq. (19) over the whole duration of the emitted field, except for the final time interval of the duration  $T_0$  at the very trailing edge of the emitted signal, where one gets a half-cycle burst identical to Eqs. (16) and (17). Therefore one obtains here the long rectangular unipolar pulse followed by an intense unipolar half-cycle burst of opposite polarity of the duration  $T_0$ . A respective example of numerical simulations is shown in Fig. 10. As one can see, the emitted field indeed consists of two sequential unipolar pulses of opposite polarity—a long low-amplitude rectangular one and a much more intense half-cycle one. It is worth noting that the total electric pulse area Eq. (1) of the emitted signal equals zero, so that no zero-frequency spectral component is produced from the considered nonlinear medium. We can thus only deal with certain parts of the emitted field exhibiting constant sign of the electric field over finite time slots, which could, however, be tuned to be long enough for required applications.

## V. CONCLUSION

We have demonstrated the generation of unipolar pulses of widely tunable profile upon the excitation of an extended layer of a resonant medium with nonlinear field coupling by a pair of ultrashort excitation pulses. As an example of such a nonlinear medium one can consider a Raman-active medium which can be efficiently described by a model of nonlinearly bonded electron and nucleus oscillators. When filtering out the high-frequency spectral components by an



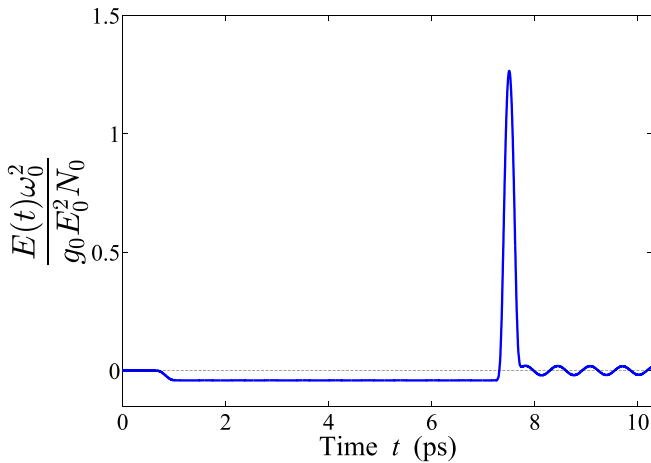


FIG. 10. Rescaled electric field obtained in reflection from an extended layer of the nonlinear resonant medium Eq. (2) with the asymmetric linearly growing profile of the spatial density distribution Eq. (26). The largest value of the density of resonant centers  $N_0 = 10^{18} \text{ cm}^{-3}$ ; the other parameters are the same as in Fig. 4.

appropriate low-pass filter, the remaining low-frequency medium response is well described by the model of a resonant medium with the nonlinear field coupling.

Two excitation pulses are selected in such a way that the time delay in between them equals half of the period of low-frequency resonant oscillations in the medium. This allows coherent control of the induced medium polarization, so that the polarization distribution represents a half cycle of the sine wave, while each molecule of the medium emits a single-cycle pulse at the medium resonant frequency. In an extended medium layer the interference of such emitted waves leads to formation of well-isolated unipolar output pulses.

The tuning of the unipolar pulse profile is achieved by adjusting the spatial density distribution of the resonant particles  $N(z)$  along the layer thickness. In particular, we have shown that rectangular- and triangular-shaped unipolar pulses can be produced for triangular and parabolic profiles of the spatial density, respectively. Paper findings therefore enable the opportunity to obtain unipolar pulses, whose temporal profile can be readily changed in a controllable way. We expect that these findings can be of significant interest for the coherent control applications, where shaping of subcycle pulses plays a crucial role to efficiently drive different ultrafast processes in matter.

#### ACKNOWLEDGMENTS

The authors acknowledge support from the Russian Science Foundation through Project No. 21-72-10028.

- 
- [1] F. Krausz and M. Ivanov, *Rev. Mod. Phys.* **81**, 163 (2009).  
 [2] U. Keller, *Appl. Phys. B* **100**, 15 (2010).  
 [3] K. Midorikawa, *Nat. Photonics* **16**, 267 (2022).  
 [4] S. Mondal, M. Shirozhan, S. Choudhary, K. Nelissen, P. Tzallas, D. Charalambidis, K. Varjú, and S. Kahaly, *Sci. Rep.* **12**, 13668 (2022).  
 [5] F. Calegari, G. Sansone, S. Stagira, C. Vozzi, and M. Nisoli, *J. Phys. B: At. Mol. Opt. Phys.* **49**, 062001 (2016).  
 [6] K. Ramasesha, S. R. Leone, and D. M. Neumark, *Annu. Rev. Phys. Chem.* **67**, 41 (2016).  
 [7] M. T. Hassan, T. T. Luu, A. Moulet, O. Raskazovskaya, P. Zhokhov, M. Garg, N. Karpowicz, A. M. Zheltikov, V. Pervak, F. Krausz, and E. Goulielmakis, *Nature (London)* **530**, 66 (2016).  
 [8] L. He, S. Sun, P. Lan, Y. He, B. Wang, P. Wang, X. Zhu, L. Li, W. Cao, P. Lu, and C. D. Lin, *Nat. Commun.* **13**, 4595 (2022).  
 [9] D. Hui, H. Alqattan, S. Yamada, V. Pervak, K. Yabana, and M. Hassan, *Nat. Photonics* **16**, 33 (2022).  
 [10] R. M. Arkipov, M. V. Arkipov, and N. N. Rosanov, *Quantum Electron.* **50**, 801 (2020).  
 [11] R. Arkipov, M. Arkipov, A. Pakhomov, I. Babushkin, and N. Rosanov, *Laser Phys. Lett.* **19**, 043001 (2022).  
 [12] N. Rosanov, *Opt. Spectrosc.* **107**, 721 (2009).  
 [13] N. N. Rosanov, R. M. Arkipov, and M. V. Arkipov, *Phys. Usp.* **61**, 1227 (2018).  
 [14] A. Wetzels, A. Gürtler, L. D. Noordam, F. Robicheaux, C. Dinu, H. G. Muller, M. J. J. Vrakking, and W. J. van der Zande, *Phys. Rev. Lett.* **89**, 273003 (2002).  
 [15] X. Chai, X. Ropagnol, S. M. Raeis-Zadeh, M. Reid, S. Safavi-Naeini, and T. Ozaki, *Phys. Rev. Lett.* **121**, 143901 (2018).  
 [16] N. Rosanov and N. Vysotina, *J. Exp. Theor. Phys.* **130**, 52 (2020).  
 [17] D. Dimitrovski, E. A. Solov'ev, and J. S. Briggs, *Phys. Rev. A* **72**, 043411 (2005).  
 [18] D. Dimitrovski, E. A. Solov'ev, and J. S. Briggs, *Phys. Rev. Lett.* **93**, 083003 (2004).  
 [19] R. M. Arkipov, A. V. Pakhomov, M. V. Arkipov, I. Babushkin, A. Demircan, U. Morgner, and N. N. Rosanov, *Opt. Lett.* **44**, 1202 (2019).  
 [20] N. Rosanov, D. Tumakov, M. Arkipov, and R. Arkipov, *Phys. Rev. A* **104**, 063101 (2021).  
 [21] A. Pakhomov, M. Arkipov, N. Rosanov, and R. Arkipov, *Phys. Rev. A* **105**, 043103 (2022).  
 [22] A. V. Bogatskaya, E. A. Volkova, and A. M. Popov, *Phys. Rev. E* **104**, 025202 (2021).  
 [23] A. V. Bogatskaya, E. A. Volkova, and A. M. Popov, *Phys. Rev. E* **105**, 055203 (2022).  
 [24] H.-C. Wu and J. Meyer-ter Vehn, *Nat. Photonics* **6**, 304 (2012).  
 [25] J. Xu, B. Shen, X. Zhang, Y. Shi, L. Ji, L. Zhang, T. Xu, W. Wang, X. Zhao, and Z. Xu, *Sci. Rep.* **8**, 2669 (2018).  
 [26] R. Pang, Y. Wang, X. Yan, and B. Eliasson, *Phys. Rev. Appl.* **18**, 024024 (2022).  
 [27] Y. Shou, R. Hu, Z. Gong, J. Yu, J.-e. Chen, G. Mourou, X. Yan, and W. Ma, *New J. Phys.* **23**, 053003 (2021).  
 [28] E. S. Efimenko, S. A. Sychugin, M. V. Tsarev, and M. I. Bakunov, *Phys. Rev. A* **98**, 013842 (2018).  
 [29] M. V. Tsarev and M. I. Bakunov, *Opt. Express* **27**, 5154 (2019).  
 [30] I. E. Ilyakov, B. V. Shishkin, E. S. Efimenko, S. B. Bodrov, and M. I. Bakunov, *Opt. Express* **30**, 14978 (2022).

- [31] M. V. Arkhipov, A. N. Tsyarkin, A. M. Zhukova, A. O. Ismagilov, A. V. Pakhomov, N. N. Rosanov, and R. M. Arkhipov, *JETP Lett.* **115**, 1 (2022).
- [32] V. P. Kalosha and J. Herrmann, *Phys. Rev. Lett.* **83**, 544 (1999).
- [33] A. Parkhomenko and S. Sazonov, *J. Exp. Theor. Phys.* **87**, 864 (1998).
- [34] X. Song, W. Yang, Z. Zeng, R. Li, and Z. Xu, *Phys. Rev. A* **82**, 053821 (2010).
- [35] V. V. Kozlov, N. N. Rosanov, C. De Angelis, and S. Wabnitz, *Phys. Rev. A* **84**, 023818 (2011).
- [36] S. Sazonov, *JETP Lett.* **114**, 132 (2021).
- [37] S. Sazonov, *Laser Phys. Lett.* **18**, 105401 (2021).
- [38] R. M. Arkhipov, M. V. Arkhipov, P. A. Belov, Y. A. Tolmachev, and I. Babushkin, *Laser Phys. Lett.* **13**, 046001 (2016).
- [39] R. M. Arkhipov, A. V. Pakhomov, I. V. Babushkin, M. V. Arkhipov, Y. A. Tolmachev, and N. N. Rosanov, *J. Opt. Soc. Am. B* **33**, 2518 (2016).
- [40] A. V. Pakhomov, R. M. Arkhipov, I. V. Babushkin, M. V. Arkhipov, Y. A. Tolmachev, and N. N. Rosanov, *Phys. Rev. A* **95**, 013804 (2017).
- [41] A. V. Pakhomov, R. M. Arkhipov, M. V. Arkhipov, A. Demircan, U. Morgner, N. N. Rosanov, and I. V. Babushkin, *Sci. Rep.* **9**, 7444 (2019).
- [42] R. M. Arkhipov, A. V. Pakhomov, M. V. Arkhipov, A. Demircan, U. Morgner, N. N. Rosanov, and I. Babushkin, *Phys. Rev. A* **101**, 043838 (2020).
- [43] V. T. Platonenko and R. V. Khokhlov, *Zh. Eksp. Teor. Fiz.* **46**, 555 (1964) [*Sov. Phys. JETP* **19**, 378 (1964)].
- [44] S. A. Akhmanov and S. Y. Nikitin, *Physical Optics* (Clarendon Press, Oxford, 1997).
- [45] A. M. Weiner, D. E. Leaird, G. P. Wiederrecht, and K. A. Nelson, *J. Opt. Soc. Am. B* **8**, 1264 (1991).
- [46] M. V. Arkhipov, R. M. Arkhipov, A. V. Pakhomov, I. V. Babushkin, A. Demircan, U. Morgner, and N. N. Rosanov, *Opt. Lett.* **42**, 2189 (2017).
- [47] L. D. Landau and E. M. Lifshitz, *The Classical Theory of Fields* (Butterworth-Heinemann, Oxford, 1980).
- [48] A. V. Pakhomov, M. V. Arkhipov, N. N. Rosanov, and R. M. Arkhipov, *JETP Lett.* **116**, 149 (2022).
- [49] B. A. Palmer, A. Le Comte, K. D. Harris, and F. Guillaume, *J. Am. Chem. Soc.* **135**, 14512 (2013).